Published for SISSA by Springer

Received: *April 5, 2025*
Revised: *September 4, 2025*
Accepted: *November 8, 2025*
Published: *December 15, 2025*

Two-loop helicity amplitudes for diphoton production with massive quark loop

Taushif Ahmed,[a] **Amlan Chakraborty**,[b,c] **Ekta Chaubey**[d] **and Mandeep Kaur**[e]

[a] *Institute for Theoretical Physics, University of Regensburg, 93040 Regensburg, Germany*
[b] *Tif Lab, Dipartimento di Fisica, Universitá di Milano, Sezione di Milano, Via Celoria 16, I-20133 Milano, Italy*
[c] *The Institute of Mathematical Sciences, 600113 Chennai, India*
[d] *Bethe Center for Theoretical Physics, Universitaet Bonn, 53115 Bonn, Germany*
[e] *Deutsches Elektronen-Synchrotron DESY, Platanenallee 6, 15738 Zeuthen, Germany*

E-mail: taushif.ahmed@ur.de, amlan.chakraborty@unimi.it, eekta@uni-bonn.de, mandeep.kaur@desy.de

Abstract: We compute two-loop helicity amplitudes in QCD for diphoton production through quark- and gluon-initiated channels, accounting for a massive internal quark loop by keeping its full mass dependence. Using physical projectors, we directly decompose the amplitude into its helicity components. By renormalising the heavy quark mass in on-shell, and other quantities in $\overline{\text{MS}}$ schemes, we obtain finite remainders. We provide benchmark values of the helicity amplitudes, expressed in terms of a canonical basis for all the non-elliptic integrals. We also present our findings through plots. The effect of a heavy quark is expected to play a crucial role in high-luminosity LHC.

Keywords: Factorization, Renormalization Group, Higher-Order Perturbative Calculations, Top Quark

ArXiv ePrint: 2502.03282

https://doi.org/10.1007/JHEP12(2025)106

Contents

1 Introduction

The production of diphotons ($\gamma\gamma$) at high-energy colliders, such as the Large Hadron Collider (LHC), serves as an important process in probing the Standard Model (SM) and exploring potential new physics [1, 2]. Diphoton final states provide a clean experimental signature due to the excellent photon identification and reconstruction capabilities in modern detectors. They also play a crucial role in precision studies, such as measuring Higgs boson properties, testing perturbative Quantum Chromodynamics (QCD), and searching for exotic particles or phenomena. The differential cross-section of this process has been precisely measured at both the Tevatron [3, 4] and the LHC [5, 6]. This signature was pivotal as one of the two "golden channels" that led to the discovery of the Higgs boson [7, 8]. The $H \to \gamma\gamma$ decay remains one of the cleanest final states for exploring the properties of the Higgs boson and its production mechanisms.

At hadron colliders, diphoton production at leading order (LO) originates from the annihilation of a quark and an antiquark via the process $q\bar{q} \to \gamma\gamma$. Corrections at next-to-LO (NLO) in the strong coupling constant (α_s) for this process were computed decades ago in ref. [9]. Subsequent developments have extended this to next-to-NLO (NNLO) accuracy ($\mathcal{O}(\alpha_s^2)$) [10–13], with results implemented in public computational tools such as 2γNNLO [10], MCFM [11], and Matrix [14]. The relevant scattering amplitudes in massless QCD have been extensively studied in refs. [15–18]. Currently, it is available up to three loops [19]. In refs. [20–23], the two-loop amplitude associated with a jet has been computed. These form a building block for next-to-NNLO (N^3LO) corrections in massless QCD. The inclusion of massive quark in the loop starts appearing only at NNLO (α_s^2) level. In ref. [11], the effect of the top quark was discussed. Recently, the full phenomenological study has been conducted in ref. [24] and the underlying two-loop helicity amplitudes have been presented in ref. [25], where the master integrals were evaluated employing generalised power series method.

JHEP12(2025)106

At NNLO, a new production channel emerges: the fusion of gluons into a diphoton pair, mediated by a quark loop, as shown in figure 1 for a massive quark. The gluon-induced contribution is not only finite and gauge-invariant on its own but also unusually significant due to the large gluon-gluon luminosity at hadron colliders. Its contribution is of the size of born subprocess $q\bar{q} \to \gamma\gamma$. Higher-order corrections to this gluon fusion channel, specifically at $\mathcal{O}(\alpha_s^3)$, involve two-loop contributions to $gg \to \gamma\gamma$. The two-loop computation for the massless QCD case was first carried out in ref. [26], while ref. [27] extended this work to include configurations involving an associated jet. Their phenomenological analysis in massless QCD was performed in [11, 28]. Currently, the amplitude is available at three-loop order [29]. Although the fully analytic two-loop amplitude for this process, including a top quark loop, has not yet been presented in the literature, its impact on the cross-section has been explored. Previous studies have relied on numerical [30] and semi-numerical [31] evaluations, with the latter incorporating analytic expressions for the subset of master integrals that were available at the time.

The *goal* of this article is to present, the computation of the two-loop amplitude for $gg \to \gamma\gamma$, retaining the full top-quark mass dependence within the loop and expressing the result as analytic coefficients of a canonical basis for all the non-elliptic integrals. The part of the amplitude containing elliptic integrals is kept as it is due to the lack of a convenient functional representation of these integrals. These integrals contribute only to the finite part of the amplitude. We also compute the two-loop amplitude for $q\bar{q} \to \gamma\gamma$ with a massive top quark in the loop, with representative diagrams shown in figure 2. The quark-initiated two-loop amplitude contributes at NNLO ($\mathcal{O}(\alpha_s^2)$), while the gluon-initiated counterpart appears at N^{3}LO ($\mathcal{O}(\alpha_s^3)$) in QCD at hadron colliders.

Representing helicity amplitudes in analytic form is not only essential for advancing our understanding of quantum field theory, but also crucial for ensuring numerical stability in cross-section computations and related observables. Such amplitudes provide a platform to compare numerical behaviour, stability, and performance with existing results, and they also serve as valuable input for evaluating cross-sections within various subtraction schemes, in particular when studying results derived from local subtraction frameworks. The virtual amplitude presented here is a key ingredient in this endeavour and will also pave the way for computing helicity amplitudes for dijet production at the LHC with the inclusion of the top-quark mass in the loop. From a technical perspective, by isolating the contributions of elliptic integrals, this work critically examines their impact on the amplitudes, thereby offering deeper insight into their analytic structure.

We adopt the method of projecting the amplitude onto the helicity basis using physical projectors, as described in refs. [32, 33]. An alternative approach to constructing physical projectors is discussed in ref. [34]. The bare integrand is generated and processed through a series of in-house codes implemented in `FORM` [35]. The associated Feynman integrals are subsequently processed through `Kira` [36, 37] to apply integration-by-parts identities (IBP) [38, 39] to express the integrand in terms of a minimal set of master integrals. These integrals have been extensively studied in the literature [24, 25, 40–43]. In ref. [44], the final missing set of master integrals containing elliptic sectors was evaluated by some of us, thereby enabling the complete analytic computation of these amplitudes. While many of these

JHEP12(2025)106

integrals exist in various forms in the literature, we independently set up a comprehensive system of differential equations containing all the occurring master integrals to ensure a consistent representation. The bare helicity amplitudes are renormalised in a mixed scheme: we adopt the on-shell scheme for mass renormalisation, while the remaining quantities are renormalised in the $\overline{\text{MS}}$. As an ancillary file [45], we provide the helicity amplitudes expressed in terms of a set of canonical master integrals. The finite remainder is available upon request from the authors for those interested. We present a few benchmark numerical values of all helicity amplitudes, in particular, around the top quark threshold. We also present plots of squared amplitudes.

The article is organised as follows. Section 2 describes the kinematic setup of the process including its Lorentz covariant decomposition. In section 3, we describe the method of constructing helicity amplitudes and the procedure to get the bare integrand. The ultraviolet renormalisation and infrared factorisation are discussed in section 4. In section 5, we discuss the results and their numerical implementation. We also describe the checks performed to ensure the correctness of the results. We conclude with our outlook in section 6.

2 Setup

We consider the following scattering processes:

$$\begin{aligned} g(p_1) + g(p_2) + \gamma(p_3) + \gamma(p_4) &\to 0\,, \\ q(p_1) + \bar{q}(p_2) + \gamma(p_3) + \gamma(p_4) &\to 0\,. \end{aligned} \tag{2.1}$$

We label the momenta of the particles by $p_1, \cdots, p_4$ and regard all of them as incoming that satisfy

$$p_1 + p_2 + p_3 + p_4 = 0\,, \qquad p_i^2 = 0. \tag{2.2}$$

The physical di-photon production at the LHC can be obtained from (2.1) by crossing $p_{3,4} \to -p_{3,4}$. In computing an observable, such as cross-section for the di-photon production, one requires $g\gamma \to g\gamma$ and $q\gamma \to q\gamma$ channels which can also be obtained by crossing from (2.1). The kinematic Mandelstam invariants of the process,

$$s = (p_1 + p_2)^2\,,\ t = (p_2 + p_3)^2\,,\ u = (p_1 + p_3)^2\,, \tag{2.3}$$

are related by momentum conservation $s + t + u = 0$. Consequently, no Euclidean region exists kinematically for the scattering process, rendering it interesting to study. The $2 \to 2$ physical region corresponds to the scattering region

$$s > 0\,, t < 0\,, u < 0\,. \tag{2.4}$$

We construct two dimensionless parameters as

$$x = \frac{s}{m_t^2}, \quad y = \frac{t}{m_t^2}, \tag{2.5}$$

where m_t denotes the mass of the top quark.

JHEP12(2025)106

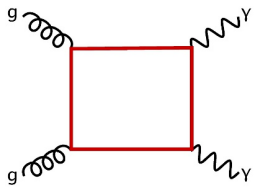

Figure 1. Representative leading order Feynman diagrams for gluon-initiated channel involving massive quark loop. The red lines represent top-quark, while the curly and wavy black lines correspond to gluon and photon, respectively.

In this article, we consider the scattering with at least one massive quark in the loop. So, both are loop-induced processes, as shown in figure 1 and 2. Our goal is to calculate the two-loop amplitude of these processes in QCD. We denote the mass of the massive quark by m_t. The amplitude can be rewritten by factoring out the overall color factors as

$$\mathcal{A}^{g|q} = \mathcal{C}^{g|q}\, A^{g|q}\,, \tag{2.6}$$

where

$$\mathcal{C}^{g} = \delta^{a_1 a_2}, \quad \mathcal{C}^{q} = \delta^{i_1 i_2} \tag{2.7}$$

for $gg \to \gamma\gamma$ and $q\bar{q} \to \gamma\gamma$, respectively. The notation $g|q$ denotes either gluon- or quark-initiated channel. Here, $i_n(a_n)$ represents an SU(N_c) index in the fundamental (adjoint) representation. The partial amplitude A depends on the number of active massless (n_f) and massive (n_{f_t}) quark flavors, as well as their respective electric charges, denoted by Q_f and Q_{f_t}. Since we focus on Feynman diagrams that include at least one massive quark loop, meaning the lowest power of n_{f_t} contributing to the amplitude is 1. After extracting all color structures, the partial amplitude can further be decomposed into a basis of $N_T^{g|q}$ independent Lorentz covariant tensor structures $T_i^{g|q}$ as

$$A^{g|q} = \sum_{i=1}^{N_T^{g|q}} \mathcal{F}_i^{g|q} T_i^{g|q}\,, \tag{2.8}$$

where $\mathcal{F}_i^{g|q}$ are called the form factors. These form factors can be expanded perturbatively in powers of the strong coupling constant, α_s.

We adopt the 't Hooft-Veltman (tHV) regularisation scheme [46], in which loop momenta are treated in $d = 4 - 2\epsilon$ dimensions, while external momenta and polarisations remain in four dimensions. Within this framework, we follow the method proposed in [32, 33], which eliminates the evanescent (-2ϵ)-dimensional helicity states and allows us to work with a set of tensors $T_i^{g|q}$ whose number corresponds directly to the independent helicity configurations. A similar approach can be found in refs. [34, 47].

In $gg \to \gamma\gamma$ channel, there are $N_T^g = 8$ independent tensor structures. By adopting the cyclic gauge choice, $\epsilon_i \cdot p_{i+1} = 0$ (with $p_5 \equiv p_1$), and applying the transversality condition,

JHEP12(2025)106

$\epsilon_i \cdot p_i = 0$, we obtain the following results [32, 33, 48, 49]:

$$
\begin{aligned}
&T_1^g = p_1{\cdot}\epsilon_2\; p_1{\cdot}\epsilon_3\; p_2{\cdot}\epsilon_4\; p_3{\cdot}\epsilon_1, && T_2^g = \epsilon_3{\cdot}\epsilon_4\; p_1{\cdot}\epsilon_2\; p_3{\cdot}\epsilon_1, && T_3^g = \epsilon_2{\cdot}\epsilon_4\; p_1{\cdot}\epsilon_3\; p_3{\cdot}\epsilon_1,\\
&T_4^g = \epsilon_2{\cdot}\epsilon_3\; p_2{\cdot}\epsilon_4\; p_3{\cdot}\epsilon_1, && T_5^g = \epsilon_1{\cdot}\epsilon_4\; p_1{\cdot}\epsilon_2\; p_1{\cdot}\epsilon_3, && T_6^g = \epsilon_1{\cdot}\epsilon_3\; p_1{\cdot}\epsilon_2\; p_2{\cdot}\epsilon_4,\\
&T_7^g = \epsilon_1{\cdot}\epsilon_2\; p_1{\cdot}\epsilon_3\; p_2{\cdot}\epsilon_4, && T_8^g = \epsilon_1{\cdot}\epsilon_2\; \epsilon_3{\cdot}\epsilon_4 + \epsilon_1{\cdot}\epsilon_4\; \epsilon_2{\cdot}\epsilon_3 + \epsilon_1{\cdot}\epsilon_3\; \epsilon_2{\cdot}\epsilon_4. && (2.9)
\end{aligned}
$$

The polarisation vector is denoted by $\epsilon(p_i) \equiv \epsilon_i$. Unlike in tHV scheme, in conventional dimensional regularisation, one requires 10 tensorial structures [50, 51]. In $q\bar{q} \to \gamma\gamma$ channel, $N_T^q = 4$ and with the gauge choice $\epsilon_3 \cdot p_2 = \epsilon_4 \cdot p_1 = 0$, we get [49, 52]

$$
\begin{aligned}
&T_1^q = \bar{u}(p_2)\not{\epsilon}_3 u(p_1)\; \epsilon_4{\cdot}p_2, && T_2^q = \bar{u}(p_2)\not{\epsilon}_3 u(p_1)\; \epsilon_4{\cdot}p_1,\\
&T_3^q = \bar{u}(p_2)\not{p}_3 u(p_1)\; \epsilon_3{\cdot}p_1\; \epsilon_4{\cdot}p_2, && T_4^q = \bar{u}(p_2)\not{p}_3 u(p_1)\; \epsilon_3{\cdot}\epsilon_4\,. && (2.10)
\end{aligned}
$$

The form factors $\mathcal{F}_i^{g|q}$ can be extracted from $A^{g|q}$ with appropriate projectors $P_j^{g|q}$, defined to satisfy the orthogonality condition $\sum_{pol} P_j^{g|q} T_i^{g|q} = \delta_{ji}$.

3 Helicity amplitudes

To compute the helicity amplitudes $A_{\vec{\lambda}}^{g|q}$, it suffices to evaluate the tensors $T_i^{g|q}$ for specific helicity configurations $\vec{\lambda} = \{\lambda_1, \lambda_2, \lambda_3, \lambda_4\}$ of the external particles. Each helicity amplitude corresponding to a given configuration $\vec{\lambda}$ can then be expressed as a linear combination of the form factors $\mathcal{F}_i^{g|q}$ as

$$
A_{\vec{\lambda}}^{g|q} = \sum_{i=1}^{N_T^{g|q}} T_{i,\vec{\lambda}}^{g|q} \mathcal{F}_i^{g|q} = \mathcal{S}_{\vec{\lambda}}^{g|q}\, \mathcal{H}_{\vec{\lambda}}^{g|q}\,. \tag{3.1}
$$

The overall spinor factors $\mathcal{S}_{\vec{\lambda}}^{g|q}$ can be extracted from $A_{\vec{\lambda}}^{g|q}$ using the spinor-helicity formalism. For a detailed introduction to this approach, we refer to ref. [53]. In this formalism, external quarks with fixed helicities are defined as

$$
|p\rangle = \overline{[p|} = \frac{1+\gamma_5}{2} u(p)\,, \quad |p] = \overline{\langle p|} = \frac{1-\gamma_5}{2} u(p)\,, \tag{3.2}
$$

with $[p| = \bar{u}(p)\frac{1-\gamma_5}{2}$ and $\langle p| = u(p)\frac{1+\gamma_5}{2}$ treating particles and anti-particles on an equal footing, while polarisation vectors take the following form

$$
\epsilon_{j,+}^{\mu} = \frac{\langle p_j|\gamma^{\mu}|q_j]}{\sqrt{2}[p_j q_j]}\,, \quad \epsilon_{j,-}^{\mu} = \frac{\langle q_j|\gamma^{\mu}|p_j]}{\sqrt{2}\langle q_j p_j\rangle}\,, \tag{3.3}
$$

where q_i is the massless reference vector corresponding to the i-th external gluon and is chosen consistently with the gauge conditions used to determine the tensor bases of eqs. (2.9) and (2.10). For the $gg \to \gamma\gamma$ channel, there are 8 independent helicity amplitudes which are related to the remaining ones through parity as

$$
A_{\vec{\lambda}}^{g} = A_{-\vec{\lambda}}^{g}(\langle ij\rangle \leftrightarrow [ji]). \tag{3.4}
$$

Here the negative sign flips the helicity. We choose independent $\vec{\lambda} = \{++++, -+++, +-++, ++-+, +++-, --++, -+-+, +--+\}$. By choosing the reference vector $q_i = p_{i+1}$, where we identify $p_5 \equiv p_1$, we have the following spinor factors [26]

$$\begin{aligned}
\mathcal{S}^g_{++++} &= \frac{\langle 12\rangle\langle 34\rangle}{[12][34]}\,, & \mathcal{S}^g_{-+++} &= \frac{[12][14]\langle 24\rangle}{[34][23][24]}\,, & \mathcal{S}^g_{+-++} &= \frac{[21][24]\langle 14\rangle}{[34][13][14]}\,,\\
\mathcal{S}^g_{++-+} &= \frac{[32][34]\langle 24\rangle}{[14][21][24]}\,, & \mathcal{S}^g_{+++-} &= \frac{[42][43]\langle 23\rangle}{[13][21][23]}\,, & \mathcal{S}^g_{--++} &= \frac{[12]\langle 34\rangle}{\langle 12\rangle[34]}\,,\\
\mathcal{S}^g_{-+-+} &= \frac{[13]\langle 24\rangle}{\langle 13\rangle[24]}\,, & \mathcal{S}^g_{+--+} &= \frac{[23]\langle 14\rangle}{\langle 23\rangle[14]}\,.
\end{aligned} \tag{3.5}$$

For the $q\bar{q} \to \gamma\gamma$ channel, we have 4 independent helicity amplitudes which can be used to obtain the remaining 4 through charge-conjugation as

$$A^q_{+-\lambda_3\lambda_4} = A^q_{-+\lambda_3^*\lambda_4^*}(\langle ij\rangle \leftrightarrow [ji])\,. \tag{3.6}$$

The λ^* refers opposite helicity of λ. We choose $q_3 = p_2,\ q_4 = p_1$ and define the spinor factors as

$$\begin{aligned}
\mathcal{S}^q_{-+--} &= \frac{2[34]^2}{\langle 13\rangle[23]}\,, & \mathcal{S}^q_{-+-+} &= \frac{2\langle 24\rangle[13]}{\langle 23\rangle[24]}\,,\\
\mathcal{S}^q_{-++-} &= \frac{2\langle 23\rangle[41]}{\langle 24\rangle[32]}\,, & \mathcal{S}^q_{-+++} &= \frac{2\langle 34\rangle^2}{\langle 31\rangle[23]}\,.
\end{aligned} \tag{3.7}$$

In our conventions, all external legs are treated as incoming. For outgoing particles, the helicities of the respective legs must be reversed. The spinor inner products are defined as $\langle ij\rangle = \langle i^-|j^+\rangle$ and $[ij] = \langle i^+|j^-\rangle$, where $|i^\pm\rangle$ represent massless Weyl spinors associated with the momentum p_i and labeled by their helicity sign. These inner products are antisymmetric and have magnitudes given by $|\langle ij\rangle| = |[ij]| = \sqrt{s_{ij}}$, where $s_{ij} = 2p_i \cdot p_j$ are the usual Mandelstam invariants: $s_{12} = s,\ s_{23} = t,\ s_{13} = u$. Consequently, the helicity-dependent factors $S^{g|q}_{\lambda_1\lambda_2\lambda_3\lambda_4}$, derived from these spinor products, are pure phases.

The spinor-free helicity amplitude $\mathcal{H}^{g|q}_{\vec{\lambda}}$ can be expanded in powers of bare strong coupling $\alpha_{s,b}$ as

$$\mathcal{H}^{g|q}_{\vec{\lambda}} = 4\pi\alpha \sum_{\ell=0}^{2} \left(\frac{\alpha_{s,b}}{4\pi}\right)^\ell \mathcal{H}^{g|q,(\ell)}_{\vec{\lambda}} + \mathcal{O}(\alpha^3_{s,b})\,, \tag{3.8}$$

where we factor out an overall term proportional to the square of the electric charge, $e^2 = 4\pi\alpha$. The quantity $\mathcal{H}^{g|q,(\ell)}_{\vec{\lambda}}$ represents the bare ℓ-loop amplitude. It is important to note that, as the $gg \to \gamma\gamma$ channel is loop-induced, the leading-order term in its perturbative expansion vanishes. In contrast, the $q\bar{q} \to \gamma\gamma$ channel contributes non-trivially to all three orders. For the quark-initiated processes involving at least one massive quark loop, non-zero diagrams begin to appear only at the two-loop level. However, through renormalization, the lower-order diagrams also contribute indirectly to the overall result.

We generate the Feynman diagrams for each channel using `Qgraf`[54]. There are 8 diagrams at one-loop for gg channel. At two loops, the gg channel comprises 166 diagrams, while the $q\bar{q}$ channel contains 55 diagrams. Samples of the two-loop diagrams are illustrated

JHEP12(2025)106

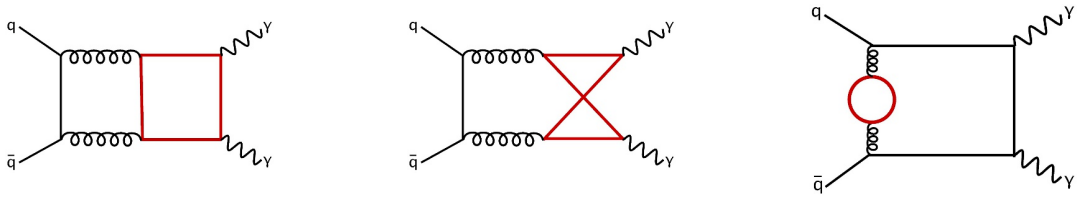

Figure 2. Representative two-loop Feynman diagrams for $q\bar{q}$ channel.

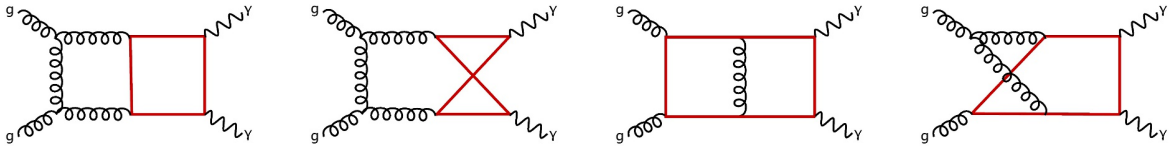

Figure 3. Representative two-loop Feynman diagrams for gg channel.

in figures 2 and 3. To process these diagrams, we use `FORM` [35], applying the tensor projectors defined in eqs. (2.9) and (2.10). We evaluate the Dirac traces and simplify the colour algebra using in-house codes. The latter involves repeated application of standard colour identities,

$$(T^a)_{ij}(T^a)_{kh} = \frac{1}{2}\left(\delta_{ih}\delta_{kj} - \frac{1}{N_c}\delta_{ij}\delta_{kh}\right), \quad f^{abc} = -2\,i\,\mathrm{Tr}(T^a[T^b,T^c])\,. \tag{3.9}$$

The form factors are expressed as linear combinations of scalar Feynman integrals, with rational coefficients that depend on the Mandelstam invariants s, t, mass m_t, and the dimensional regulator ϵ. The form factors for the $gg \to \gamma\gamma$ process involve 26,577 scalar Feynman integrals, while the $q\bar{q} \to \gamma\gamma$ process requires 2,289 integrals. We parametrize the ℓ-loop Feynman integrals as follows:

$$I^{\text{top}}_{n_1,n_2,\ldots,n_N} = \mu_0^{2L\epsilon} e^{L\epsilon\gamma_E} \int \prod_{i=1}^{L} \left(\frac{\mathrm{d}^d k_i}{i\pi^{\frac{d}{2}}}\right) \frac{1}{D_1^{n_1} D_2^{n_2} \ldots D_N^{n_N}}. \tag{3.10}$$

The superscript "top" refers to any of the integral families mentioned below. Here, $\gamma_E = 0.5772\ldots$ is the Euler-Mascheroni constant, and μ_0 is the dimensional regularization scale. The factor $e^{L\epsilon\gamma_E}$ is purely conventional and is chosen for later convenience, while the factor $\mu_0^{2L\epsilon}$ ensures that the integrals maintain integer mass dimensions. For a general process with E independent external momenta and L loops, one requires $L(L+1)/2 + LE$ independent denominators to describe all possible scalar products of loop momenta with either loop or external momenta. A specific complete set of denominators D_i at a given loop order is typically referred to as an integral family. We organize the amplitude into as few integral families as possible, allowing for permutations of external momenta (crossings). At two loops, this requires two planar and two non-planar families, which we present in tabular form in table 1. There, we indicate the loop momenta with k_1 and k_2. We name PL1 and PL2 the families corresponding to the planar graphs and NPL1, NPL2 the ones corresponding to the non-planar graphs. We present the top sector diagrams for each integral family in figure 4.

The integrals appearing in the form factors are not all linearly independent. To identify symmetry relations among the integrals, we employ `Reduze2` [55, 56]. Subsequently, we use `Kira` [36, 37] and `LiteRed` [57], which are implementations of the Laporta algorithm [58], and

JHEP12(2025)106

Family	PL1	PL2	NPL1	NPL2
D_1	$k_1^2 - m_t^2$	k_1^2	k_1^2	$(k_1 - p_1)^2$
D_2	$(k_1 + p_1)^2 - m_t^2$	$(k_1 + p_1)^2$	$(k_1 + p_1)^2$	k_1^2
D_3	$(k_1 + p_1 + p_2)^2 - m_t^2$	$(k_1 + p_1 + p_2)^2$	$(k_1 + k_2)^2 - m_t^2$	$(k_1 + p_2)^2$
D_4	$(k_1 + k_2)^2$	$(k_1 + k_2)^2 - m_t^2$	$k_2^2 - m_t^2$	$(k_1 + k_2 - p_1)^2 - m_t^2$
D_5	$k_2^2 - m_t^2$	$k_2^2 - m_t^2$	$(k_2 + p_3)^2 - m_t^2$	$k_2^2 - m_t^2$
D_6	$(k_2 + p_3)^2 - m_t^2$	$(k_2 + p_3)^2 - m_t^2$	$(k_2 - p_1 - p_2)^2 - m_t^2$	$(k_2 + p_3)^2 - m_t^2$
D_7	$(k_2 - p_1 - p_2)^2 - m_t^2$	$(k_2 - p_1 - p_2)^2 - m_t^2$	$(k_1 + k_2 - p_2)^2 - m_t^2$	$(k_1 + k_2 + p_2 + p_3)^2 - m_t^2$
D_8	$(k_2 - p_1)^2 - m_t^2$	$(k_2 - p_1)^2 - m_t^2$	$(k_2 - p_1)^2 - m_t^2$	$(k_1 + p_3)^2$
D_9	$(k_1 - p_3)^2 - m_t^2$	$(k_1 - p_3)^2$	$(k_1 + p_3)^2$	$(k_2 - p_1)^2 - m_t^2$

Table 1. Planar and non-planar integral families at two loops. The first seven entries denote the real propagators appearing in Feynman diagrams. All diagrams are mapped to these and their crossed families.

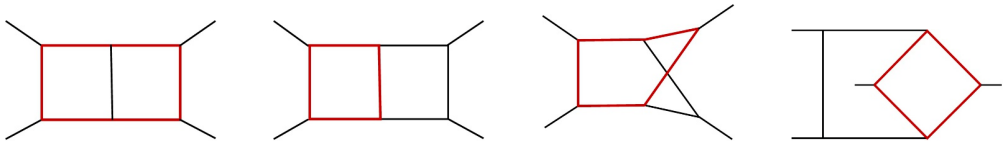

Figure 4. Topology diagrams respectively for PL1, PL2, NPL1, NPL2 in the top sector. Red lines represent massive particles, while black lines denote massless ones.

`FiniteFlow` [59], to solve integration-by-parts (IBP) relations. This algorithm leverages finite field arithmetic [59–62] to systematically reduce the integrals to a minimal, independent basis set of master integrals (MIs). Specifically, we obtain 29 MIs in PL1, 32 in PL2, 54 in NPL1, and 36 in NPL2. The required master integrals for the amplitudes correspond to the families {PL1, PL2, NPL1 and NPL2} and their crossings: $\{p_1 \leftrightarrow p_2\}$, $\{p_1 \to p_2, p_2 \to p_3, p_3 \to p_1\}$, $\{p_1 \to p_2, p_2 \to p_4, p_4 \to p_1\}$, $\{p_1 \to p_2, p_2 \to p_3, p_3 \to p_4, p_4 \to p_1\}$ and $\{p_1 \to p_2, p_2 \to p_4, p_4 \to p_3, p_3 \to p_1\}$. Taking into account all crossings, we find 65 master integrals for the $q\bar{q}$ channel and 171 for the gg channel.

For this independent set of uncrossed master integrals, we employ the method of differential equations to find a *good* basis. Using IBP identities, we establish a unified system of differential equations for these MIs with respect to both Mandelstam variables s and t (with m_t set to 1 for simplification). The system attains the form

$$d\vec{I}^{\text{top}} = (dM)\vec{I}^{\text{top}}, \tag{3.11}$$

where M is an 88×88 matrix depending rationally on Mandelstam variables s, t, and dimensional regulator ϵ.

In our case study, the uncrossed integrals, belonging to the families {PL1, PL2, NPL1, NPL2}, have been extensively studied in different contexts [24, 25, 40–43], and are well known to satisfy an ϵ-factorized differential equation system [63]. Consequently, our choice of the pre-canonical basis for these integrals follows the work in refs. [41–43], with some modifications. To transform the differential equation system into the ϵ-form, we employ the Magnus series expansion [64] to compute the rotation matrix for our pre-canonical basis. Furthermore, we validate the canonical basis choice for the contributing crossings by independently deriving

JHEP12(2025)106

their differential equations and obtaining the ϵ-form of the system using the corresponding mapping relations within the uncrossed setup.

The last 6 integrals in our chosen basis, which belong to the top and sub-top sectors of the non-planar family NPL2, exhibit more intricate mathematical structures. These integrals are known to involve geometries beyond multiple polylogarithms, such as elliptic curves, making their analytic solutions significantly more challenging. Recently, analytic solutions for these non-planar topologies involving elliptic sectors have become available [44] by some of us. This was the final missing piece required to express the two-loop amplitudes for diphoton production in terms of analytic functions.

With this, the choice of the canonical basis up to top and sub-top sectors of the NPL2 integrals enables a compact expression of the amplitudes across all crossings, following the mappings outlined earlier. We provide the canonical basis choice as an auxiliary file with this paper. In ref. [65], an alternative choice of canonical master integrals has been presented.

Another crucial aspect of master integral computation is their numerical evaluation across the entire physical phase-space region. Polylogarithmic integrals can be evaluated numerically in multiple ways. For instance, integrals expressible in terms of Goncharov polylogarithms can be evaluated using GINAC [66], while numerically evaluating one-fold integrals over polylogarithmic kernels, also known as dlog one-forms, as done in [42] provides another option. Similarly, the numerical evaluation of elliptic kernels can be achieved by series expanding the corresponding kernels along suitable paths in the physical phase-space region, as demonstrated in [67, 68]. The formulation of these integrals in a function basis suitable for numerical evaluation across all phase-space regions is left for future work.

4 Ultraviolet and infrared structures

The result of the computation described in the previous section are the divergent helicity amplitudes for the processes described in eq. (2.1) in terms of bare $\alpha_{s,b}$ and bare top mass $m_{t,b}$. In the following, we describe the ultraviolet (UV) renormalisation and infrared (IR) subtraction of the divergent amplitudes.

4.1 UV renormalisation

For UV singularity, we renormalise the amplitude using the modified minimal subtraction ($\overline{\text{MS}}$) scheme, except for the top quark mass, which we choose to renormalise in the on-shell (OS) scheme. The bare coupling $\alpha_{s,b}$ is written in terms of the renormalised coupling $\alpha_s(\mu)$ as

$$\alpha_{s,b}\,\mu_0^{2\epsilon}\,S_\epsilon = \alpha_s\,\mu^{2\epsilon} Z_\alpha(\alpha_s(\mu)), \tag{4.1}$$

where $S_\epsilon = (4\pi)^\epsilon e^{-\gamma_E \epsilon}$, and μ is the renormalization scale, which we set equal to μ_0. Z_α is the renormalisation constant for the strong coupling. The latter is introduced in dimensional regularisation to make the coupling constant dimensionless. The bare top-quark mass, $m_{t,b}$, is expressed in terms of the renormalized mass, m_t, as:

$$m_{t,b} S_\epsilon = m_t Z_{m_t}, \tag{4.2}$$

JHEP12(2025)106

where Z_{m_t} is the mass renormalization constant. Similarly, the bare gluon field, $\mathcal{G}_{\nu,b}$, is related to the renormalized gluon field, $\mathcal{G}_\nu$, via:

$$\mathcal{G}_{\nu,b} S_\epsilon = \mathcal{G}_\nu Z_g, \tag{4.3}$$

where Z_g is the gluon field renormalization constant. This arises due to the presence of massive quark. The bare quark field, Q_b, is connected to the renormalized one, Q, as:

$$Q_b S_\epsilon = Q Z_q, \tag{4.4}$$

where Z_q represents the quark field renormalization constant. We set $n_f = 0$ as there are no massless quark loops contributing to the processes described in eq. (2.1) at the perturbative order considered.

Gluon channel. Since the leading-order $gg \to \gamma\gamma$ amplitude is loop-induced, as shown in figure 1, it is free from both ultraviolet (UV) and infrared (IR) divergences. At two-loop level, however, the amplitude exhibits both UV and IR divergences. Notably, only a single massive quark loop contributes to the amplitude — photons can only emit from massive quarks. In other words, the two-loop amplitude does not depend on massless quarks. Therefore, we can safely disregard the massless quark contributions from the leading order when constructing the UV and IR subtraction terms. The UV renormalized helicity amplitude, $\mathcal{H}^{g,(l)}_{\vec{\lambda},\text{ren}}$ with $l = \{1, 2\}$, is obtained from the bare helicity amplitude defined in eq. (3.8) using the following:

$$\begin{aligned}
\mathcal{H}^{g,(1)}_{\vec{\lambda},\text{ren}} &= \mathcal{H}^{g,(1)}_{\vec{\lambda}}, \\
\mathcal{H}^{g,(2)}_{\vec{\lambda},\text{ ren}} &= \mathcal{H}^{g,(2)}_{\vec{\lambda}} + \left(\frac{n_g}{2}\delta Z_g + \delta Z_\alpha\right) \mathcal{H}^{g,(1)}_{\vec{\lambda},\text{ren}} + \delta Z_{m_t}\, \mathcal{H}^{g,CT,(1)}_{\vec{\lambda}}.
\end{aligned} \tag{4.5}$$

Here the renormalisation constants are expanded according to $Z_i = 1 + \left(\frac{\alpha_s}{4\pi}\right) \delta Z_i + \mathcal{O}(\alpha_s^2)$ for $i = \{\alpha, g, m_t\}$ with

$$\begin{aligned}
\delta Z_\alpha &= -\frac{\beta_0}{\epsilon} + \left(\frac{\mu^2}{{m_t}^2}\right)^\epsilon \left(\frac{4}{3\epsilon} T_F\right) n_{f_t}\,, \\
\delta Z_g &= -\left(\frac{\mu^2}{{m_t}^2}\right)^\epsilon \left(\frac{4}{3\epsilon} T_F\right) n_{f_t}\,, \\
\delta Z_{m_t} &= -\left(\frac{\mu^2}{{m_t}^2}\right)^\epsilon C_F \left(\frac{3}{\epsilon} + 4\right)\,.
\end{aligned} \tag{4.6}$$

The number of gluons in the external states is denoted by n_g which is equal to 2 in our case. The quadratic Casimir in the fundamental representation of SU(N) is $C_F = (N^2 - 1)/(2N)$, and in the adjoint representation, it is denoted by C_A. The constant T_F is defined as $T_F = 1/2$, and the leading-order β function is given by $\beta_0 = (11C_A - 2n_f)/3$. It is noteworthy that the top-mass-dependent contributions to the α_s expansions from δZ_α and δZ_g cancel each other. The counter-term amplitude for the top mass renormalization is represented by $\mathcal{H}^{g,CT,(1)}_{\vec{\lambda}}$. This counter-term amplitude is derived by inserting the mass counter-term, $\mathcal{P}^{m_t}_{ac}$, defined through

$$\mathcal{P}^{m_t}_{ac} = \frac{i\,\delta_{ab}}{\not{p} - m_t} \left(-i\,\delta Z_{m_t}\right) \frac{i\,\delta_{bc}}{\not{p} - m_t}, \tag{4.7}$$

JHEP12(2025)106

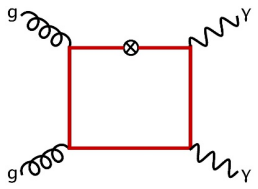

Figure 5. Sample diagram for calculating mass counter term.

into each top quark propagator in the leading-order amplitude, and collecting the coefficient of α_s^2. This can be visualised through figure 5. Alternatively, the counter-term can be computed by differentiating the leading-order amplitude with respect to m_t. This approach yields results that are in perfect agreement with the previously derived counter-term.

Quark channel. In the quark-initiated channel, one-loop diagrams containing a single massive quark loop exist but vanish due to Furry's theorem. Non-zero contributions begin to appear only at the two-loop level. These contributions can be categorized into two types of diagrams, depending on whether the photons are emitted from massive or massless quarks, as illustrated in figure 2. The first type, where photons are emitted from massive quarks, is UV and IR finite. This behaviour is expected since no such diagrams exist at lower loop levels. The second type, involving photons emitted from massless quarks, is UV divergent but IR finite. Calculating the counterterms requires considering tree-level and one-loop diagrams without massive quark involvement. Thus, while we focus on diagrams with at least one massive quark loop, the two-loop UV and IR subtraction contributions also include contributions from massless quarks which are not forming closed loops.

We split the helicity amplitude defined in eq. (3.8) with respect to the type of quarks from which the di-photon are emitted:

$$\mathcal{H}_{\vec{\lambda}}^{q,(\ell)} = Q_f^2 \, \mathcal{H}_{\vec{\lambda}}^{f,(\ell)} + \sum_{f_t=1}^{n_{f_t}} Q_{f_t}^2 \, \mathcal{H}_{\vec{\lambda}}^{f_t,(\ell)}. \tag{4.8}$$

The terms $\mathcal{H}_{\vec{\lambda}}^{f,(\ell)}$ and $\mathcal{H}_{\vec{\lambda}}^{f_t,(\ell)}$ represent the contributions from diagrams where the diphoton is emitted by massless and massive quarks, respectively. Notably, there are no non-zero mixed diagrams up to two loops. As previously mentioned, the contribution $\mathcal{H}_{\vec{\lambda}}^{f_t,(2)}$ is both UV and IR finite, because it first arises at the two-loop level. On the other hand, the contribution $\mathcal{H}_{\vec{\lambda}}^{f,(2)}$ is UV divergent but remains IR finite. In QCD, n_{f_t} equals 1.

Additionally, we require massless quark field renormalisation constants up to order α_s^2 along with the constants of eq. (4.6):

$$Z_q = 1 + \left(\frac{\alpha_s}{4\pi}\right) \delta {Z_q}^{(1)} + \left(\frac{\alpha_s}{4\pi}\right)^2 \delta Z_q^{(2)} + \mathcal{O}(\alpha_s^3), \tag{4.9}$$

with

$$\begin{aligned} \delta Z_q^{(1)} &= 0, \\ \delta Z_q^{(2)} &= \left(\frac{\mu^2}{{m_t}^2}\right)^{\epsilon} C_F \, n_{f_t} \left(\frac{1}{4\epsilon} - \frac{5}{4}\right). \end{aligned} \tag{4.10}$$

JHEP12(2025)106

We need to consider only $\mathcal{H}^{f,(\ell)}_{\vec{\lambda}}$ for renormalisation and we obtain the UV finite amplitude $\mathcal{H}^{f,(2)}_{\vec{\lambda},\text{ren}}$ by

$$\mathcal{H}^{f,(2)}_{\vec{\lambda},\text{ren}} = \mathcal{H}^{f,(2)}_{\vec{\lambda}} + \delta Z_q{}^{(1)} \mathcal{H}^{f,(1)}_{\vec{\lambda}} + \delta Z_\alpha \mathcal{H}^{f,(1)}_{\vec{\lambda}} + \delta Z_q^{(2)} \mathcal{H}^{f,(0)}_{\vec{\lambda}}. \tag{4.11}$$

$\mathcal{H}^{f,(0)}_{\vec{\lambda}}$ is tree level and $\mathcal{H}^{f,(1)}_{\vec{\lambda}}$ is the one loop helicity amplitude setting n_f to zero in $q\bar{q} \to \gamma\gamma$ channel, respectively.

4.2 IR factorisation

The IR singularity structure of QCD amplitudes has been studied up to three loops for the massless cases in refs. [69–78]. It also has been extended to the cases involving massive partons at two loops in refs. [79–83] and up to three loops [84] involving one massive parton in the external states. The IR divergences can be subtracted from our UV renormalized amplitudes, $\mathcal{H}_{\vec{\lambda},\,\text{ren}}$, multiplicatively through

$$\mathcal{H}^{g|q}_{\vec{\lambda},\,\text{fin}} = \lim_{\epsilon\to 0} \left[\mathcal{Z}_{\text{IR}}^{-1} \mathcal{H}^{g|q}_{\vec{\lambda},\,\text{ren}} \right]_{\alpha_s^{QCD} \to \xi\alpha_s}, \tag{4.12}$$

resulting IR finite $\mathcal{H}^{g|q}_{\vec{\lambda},\,\text{fin}}$. Here α_s denotes the strong coupling constant in the effective theory with $n_f = 5$ in which the heavy quark is integrated out. While considering an amplitude with heavy quark mass dependence, one must relate the α_s^{QCD}, the strong coupling constant of full QCD with $n_f = 6$ through the decoupling relation [85], $\alpha_s^{QCD} = \xi\alpha_s$. Where the ξ to the order of α_s is given by

$$\xi = 1 + \left(\frac{\alpha_s}{4\pi}\right) \sum_{i=1}^{n_{f_t}} \frac{2}{3} \left[e^{\epsilon\gamma_E}\, \Gamma(\epsilon) \left(\frac{\mu^2}{m_i^2}\right)^{\epsilon} - \frac{1}{\epsilon} \right]. \tag{4.13}$$

Here, $\mathcal{Z}_{\text{IR}}$ is a matrix in SU(N) color space acting on the space spanned by the $\mathcal{C}_i$ basis vectors (2.7) and $\mathcal{H}^{g|q}_{\vec{\lambda},\,\text{fin}}$ are finite remainders, also called hard scattering functions. The matrix $\mathcal{Z}_{\text{IR}}$ can be written as

$$\mathcal{Z}_{\text{IR}} = \mathbb{P} \exp\left[\int_\mu^\infty \frac{\mathrm{d}\mu'}{\mu'} \mathbf{\Gamma}(\{p\}, \alpha_s, \mu') \right], \tag{4.14}$$

where $\mathbb{P}$ denotes the path-ordering of color operators [74] in increasing values of μ' from left to right. The anomalous dimension matrix $\mathbf{\Gamma} = \mathbf{\Gamma}_{\text{dipole}}$ can be written as

$$\mathbf{\Gamma}_{\text{dipole}}(\{p\}, \alpha_s, \mu) = \sum_{1\le i<j\le 2} \mathbf{T}_i \cdot \mathbf{T}_j\, \gamma^{\text{K}}(\alpha_s)\, \log\left(\frac{\mu^2}{-s_{ij} - i\delta}\right) + \sum_{i=1}^{2} \gamma^i(\alpha_s)\,, \tag{4.15}$$

where $\gamma^{\text{K}}(\alpha_s)$ is the cusp anomalous dimension [86–91] and γ^i is the quark (gluon) collinear anomalous dimension [92–95] of the i-th external particle. Further, $\mathbf{T}_i^a$ represents the color generator of the i-th parton in the scattering amplitude,

$$\begin{aligned}
(\mathbf{T}_i^a)_{\alpha\beta} &= t^a_{\alpha\beta} && \text{for a final(initial)-state quark (anti-quark),}\\
(\mathbf{T}_i^a)_{\alpha\beta} &= -t^a_{\beta\alpha} && \text{for a final(initial)-state anti-quark (quark),}\\
(\mathbf{T}_i^a)_{bc} &= -if^{abc} && \text{for a gluon.}
\end{aligned} \tag{4.16}$$

As the processes, we considered in (2.1) do not have any massive parton in the external states, we exclude the contributions from massive parton in the external states in (4.15). We expand the finite remainders in powers of α_s as

$$\mathcal{H}^{g|q}_{\vec{\lambda},\text{fin}} = \sum_{\ell\geq 0}\left(\frac{\alpha_s}{4\pi}\right)^{\ell}\mathcal{H}^{g|q,(\ell)}_{\vec{\lambda},\text{fin}}\,. \tag{4.17}$$

As previously mentioned, the $q\bar{q}\to\gamma\gamma$ does not exhibit any IR divergences. We need IR subtraction only for the $gg\to\gamma\gamma$ channel. The finite remainders for the quark-initiated channel are denoted through $\mathcal{H}^{f,(l)}_{\vec{\lambda},\,\text{fin}}$ and $\mathcal{H}^{f_t,(l)}_{\vec{\lambda},\,\text{fin}}$. For the gluon-initiated channel, the corresponding expressions are given by

$$\begin{aligned}\mathcal{H}^{g,(0)}_{\vec{\lambda},\,\text{fin}} &= \mathcal{H}^{g,(0)}_{\vec{\lambda}}\,,\\ \mathcal{H}^{g,(1)}_{\vec{\lambda},\,\text{fin}} &= \mathcal{H}^{g,(1)}_{\vec{\lambda},\,\text{ren}} - \mathcal{Z}^{(1)}_{\text{IR}}\mathcal{H}^{g,(0)}_{\vec{\lambda},\,\text{ren}},\end{aligned} \tag{4.18}$$

where $\mathcal{Z}^{(n)}_{\text{IR}}$ are the coefficients of the expansion of $\mathcal{Z}_{\text{IR}}$ in α_s [74, 96]:

$$\mathcal{Z}^{(0)}_{\text{IR}} = 1\,,\qquad \mathcal{Z}^{(1)}_{\text{IR}} = \frac{\Gamma'_0}{4\epsilon^2} + \frac{\mathbf{\Gamma}_0}{2\epsilon}\,.$$

The quantities Γ'_0 and $\mathbf{\Gamma}_0$ are defined through

$$\mathbf{\Gamma}_{\text{dipole}} = \sum_{n=0}^{\infty}\mathbf{\Gamma}_n\left(\frac{\alpha_{\text{s}}}{4\pi}\right)^{n+1},\quad \Gamma' = \frac{\partial\mathbf{\Gamma}_{\text{dipole}}}{\partial\log\mu} = -\gamma^{\text{K}}\sum_i C_i = \sum_{n=0}^{\infty}\Gamma'_n\left(\frac{\alpha_{\text{s}}}{4\pi}\right)^{n+1}. \tag{4.19}$$

5 Results, checks and benchmarks

Upon including the UV counterterms, we confirm the complete cancellation of UV divergences. While not all amplitudes under consideration exhibit IR divergences, for those that do, the soft and collinear singularities align precisely with theoretical predictions, as described in section 4. This consistency is reflected in the finiteness of $\mathcal{H}^{g|q}_{\vec{\lambda},\text{fin}}$ in eq. (4.12). This agreement serves as a crucial validation of our calculation. An independent calculation of the helicity amplitudes is carried out in ref. [65], and we find perfect numerical agreements with their bare results.[1] Furthermore, we find that, in our chosen integral representations, the amplitudes in both channels contain no crossings of elliptic integrals, with the elliptic contributions isolated to only six integrals across the whole amplitudes.

As previously mentioned, due to the lack of a suitable functional basis for elliptic integrals, we use AMFlow [97, 98] to calculate finite remainders numerically at some kinematic points. In an alternative approach, in ref. [99], it has been shown that the combination of the expansion in high-energy and around the forward limit approximate the exact results to high precision. To systematically represent these results, we parameterise the physical kinematic space as [25].

$$s>0, t=-\frac{s}{2}(1-\cos\,\theta), -s<t<0. \tag{5.1}$$

[1] In conventions of this article, we observed complete agreement at the phase-space points, $(s,t,m_t) = (13/10,-3/5,1)$, $(s,t,m_t) = (11/3,-5/2,1)$ and $(s,t,m_t) = (51/10,-11/10,1)$, after adjusting for an overall factor of $1/\Gamma(1+\epsilon)^2$.

Helicity	Finite remainder
$\mathcal{H}^{f,(2)}_{-+--,\text{fin}}$	0.0003077743812
$\mathcal{H}^{f,(2)}_{-+-+,\text{fin}}$	0.3343545752627 + 0.0045759197604 I
$\mathcal{H}^{f,(2)}_{-++-,\text{fin}}$	0.3340355600039 + 0.0039728945978 I
$\mathcal{H}^{f,(2)}_{-+++,\text{fin}}$	-0.0003077743812
$\mathcal{H}^{f_t,(2)}_{-+--,\text{fin}}$	-0.0032890203623 + 0.0018737139979 I
$\mathcal{H}^{f_t,(2)}_{-+-+,\text{fin}}$	0.0149015345327 - 0.0980611917183 I
$\mathcal{H}^{f_t,(2)}_{-++-,\text{fin}}$	0.0145075046945 - 0.1001008144487 I
$\mathcal{H}^{f_t,(2)}_{-+++,\text{fin}}$	0.0032890203623 - 0.0018737139979 I

Table 2. Benchmarks for the finite remainders for the quark channel for $\theta = \frac{\pi}{6}$, $s = 3\,\text{GeV}$ and $N = 3$.

Helicity	Finite remainder
$\mathcal{H}^{g,(2)}_{++++,\text{fin}}$	-4.2353936830803 + 44.7462828017996 I
$\mathcal{H}^{g,(2)}_{-+++,\text{fin}}$	-0.2195377488355 + 0.5883781474135 I
$\mathcal{H}^{g,(2)}_{+-++,\text{fin}}$	-0.2195377488355 + 0.5883781474135 I
$\mathcal{H}^{g,(2)}_{++-+,\text{fin}}$	-0.3559355594652 + 0.1940038446546 I
$\mathcal{H}^{g,(2)}_{+++-,\text{fin}}$	-0.3559355594652 + 0.1940038446546 I
$\mathcal{H}^{g,(2)}_{--++,\text{fin}}$	0.9197367315469 - 69.8007699134945 I
$\mathcal{H}^{g,(2)}_{-+-+,\text{fin}}$	67.2257429520241 - 69.2863625098377 I
$\mathcal{H}^{g,(2)}_{+--+,\text{fin}}$	0.4096925658652 - 0.4161420588004 I

Table 3. Benchmarks for the finite remainders for the gluonic channel for $\theta = \frac{\pi}{6}$, $s = 3\,\text{GeV}$ and $N = 3$.

The scattering angle in the partonic centre of mass frame is denoted by $\theta \in (0, \pi)$. Table 2 and 3 provide benchmark values for the two-loop finite remainders of all helicity amplitudes at selected kinematic points in the physical phase space.

The existence of Bose symmetry due to the exchange of final state photons, $p_3 \leftrightarrow p_4$ is evident from the finite remainder for both quark and gluon-initiated processes. For the $q\bar{q}$ channel, it gets translated to

$$\begin{aligned}\mathcal{H}^{f|f_t,(2)}_{-+--,\text{fin}}(s,t) &= -\mathcal{H}^{f|f_t,(2)}_{-+++,\text{fin}}(s,t),\\ \mathcal{H}^{f|f_t,(2)}_{-+-+,\text{fin}}(s,t) &= \mathcal{H}^{f|f_t,(2)}_{-++-,\text{fin}}(s,u).\end{aligned} \tag{5.2}$$

JHEP12(2025)106

The notation $f|f_t$ signifies that the relations hold for both types of finite remainders. These validations serve as crucial consistency checks on our final results. For the gluon-initiated amplitude, the Bose-symmetry under the exchange of $p_1 \leftrightarrow p_2$ and/or $p_3 \leftrightarrow p_4$ implies

$$\begin{aligned}\mathcal{H}^{g,(2)}_{\lambda_1,\lambda_2,\lambda_3,\lambda_4,\text{fin}}(s,t) &= \mathcal{H}^{g,(2)}_{\lambda_2,\lambda_1,\lambda_3,\lambda_4,\text{fin}}(s,u)\\ \mathcal{H}^{g,(2)}_{\lambda_1,\lambda_2,\lambda_3,\lambda_4,\text{fin}}(s,t) &= \mathcal{H}^{g,(2)}_{\lambda_1,\lambda_2,\lambda_4,\lambda_3,\text{fin}}(s,u)\,.\end{aligned} \tag{5.3}$$

The finite remainders are checked to exhibit this symmetry. We provide the bare helicity amplitudes expressed in terms of a set of canonical master as an ancillary file [45]. The finite remainder is available upon request from the authors.

The finite remainder is a vector in colour and helicity space, which can be written as

$$\mathcal{A}^{g|q}_{\text{fin}} = \mathcal{C}^{g|q} A^{g|q}_{\text{fin}} = 4\pi\alpha\, \mathcal{C}^{g|q} \sum_{l=0} \left(\frac{\alpha_s}{4\pi}\right)^{\ell} A^{g|q,(\ell)}_{\text{fin}}\,. \tag{5.4}$$

The colour factors $\mathcal{C}^{g|q}$ correspond to the gluon and quark channels, respectively, as defined in (2.7). The interference between the finite remainders at ℓ- and ℓ'-loops can be composed out of helicity amplitudes through

$$\overline{A^{g|q,(\ell)}_{\text{fin}}} A^{g|q,(\ell')}_{\text{fin}} = \mathcal{N} \sum_{\lambda} \left(\mathcal{C}^{g|q}\right)^{\dagger} \mathcal{C}^{g|q}\, |S_\lambda|^2\, \mathcal{H}^{g|q,(\ell)*}_{\lambda,\,\text{fin}} \mathcal{H}^{g|q,(\ell')}_{\lambda,\,\text{fin}}, \tag{5.5}$$

In figure 6, we present these interferences of amplitudes for both channels.

6 Conclusions

We compute the two-loop QCD helicity amplitudes for $gg \to \gamma\gamma$ and $q\bar{q} \to \gamma\gamma$, retaining the full dependence on the top quark mass inside the loop. Using a combination of in-house and publicly available codes, we express the integrand in terms of a set of canonical master integrals except the elliptic integrals. A recent computation by some of us [44] involving a non-planar integral family with elliptic sectors provides the final missing ingredient, allowing us to complete this calculation. While the remaining required master integrals exist in the literature, we perform an independent validation by constructing a comprehensive system of differential equations encompassing all master integrals including crossings. This ensures a consistent representation of the solutions in terms of a unified set of variables. This set of uncrossed families and the corresponding function basis remain the same for dijet production. Therefore, while we defer the publication of these results to future work, we provide the bare amplitudes in terms of a chosen set of master integrals as an ancillary file [45] with this article.

We renormalise the heavy quark mass in the on-shell scheme, while other quantities are renormalised in the $\overline{\text{MS}}$ scheme. In addition to verifying the expected UV and IR divergences, we cross-check our bare amplitudes with an independent calculation by another group [65], finding complete numerical agreement at multiple physical phase-space points. We present a few benchmark values for the finite remainders for all helicity amplitudes.

These amplitudes provide a valuable input for computing cross-sections and other key observables using various subtraction schemes. It will be interesting to investigate the impact of these analytic results by comparing them with existing calculations of the diphoton

JHEP12(2025)106

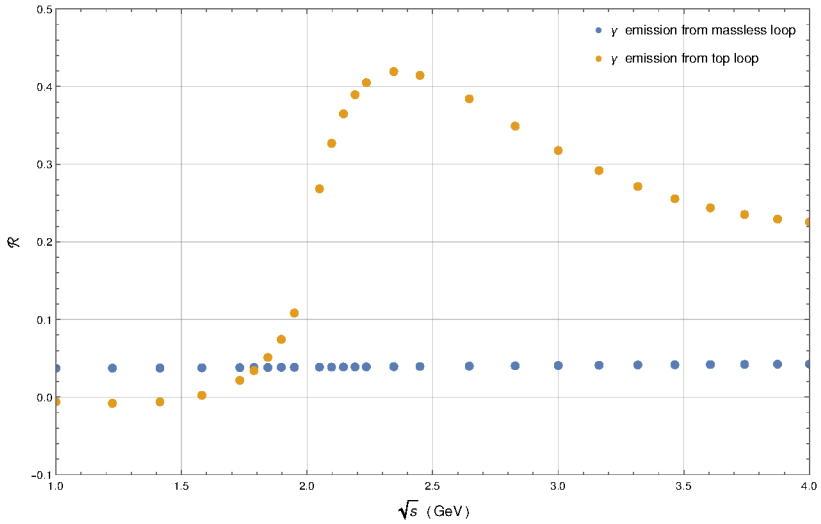

(a) Quark channel with $\mathcal{R} = \alpha_s^2 \frac{2\mathrm{Re}\left(\overline{A_{\mathrm{fin}}^{q,(0)}} A_{\mathrm{fin}}^{q,(2)}\right)}{\overline{A_{\mathrm{fin}}^{q,(0)}} A_{\mathrm{fin}}^{q,(0)}}$ on the vertical and $\sqrt{s}$ on the horizontal axis.

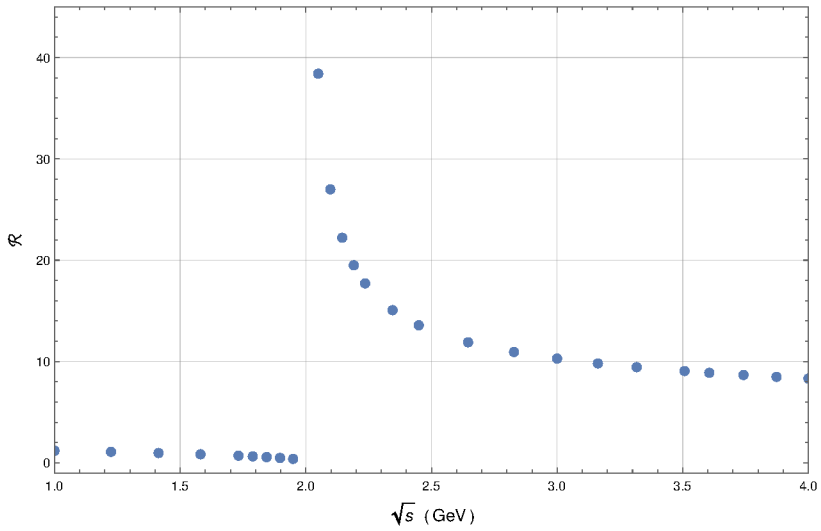

(b) Gluon channel with $\mathcal{R} = \alpha_s \frac{2\mathrm{Re}\left(\overline{A_{\mathrm{fin}}^{g,(1)}} A_{\mathrm{fin}}^{g,(2)}\right)}{\overline{A_{\mathrm{fin}}^{g,(1)}} A_{\mathrm{fin}}^{g,(1)}}$ on the vertical and $\sqrt{s}$ on the horizontal-axis.

Figure 6. Two-loop amplitudes interfered with the corresponding leading-order contributions as a function of the centre of mass energy for the processes $q\bar{q} \to \gamma\gamma$ and $gg \to \gamma\gamma$ respectively. The interference term is normalized with respect to the leading-order contribution. For the photon emitted from massive quark in quark channel, we use top and bottom for the massive and massless quarks, respectively. The mass of top quark is assumed to be unity.

JHEP12(2025)106

production cross-section for $gg \to \gamma\gamma$, where the relevant integrals were previously evaluated numerically [30] or semi-numerically [31]. The impact of the top quark mass at the high-luminosity phase of the LHC will be particularly interesting to explore, as its effects are expected to be significantly enhanced in this regime. Furthermore, this work lays the groundwork for future studies, including dijet production with a massive quark loop.

Acknowledgments

TA and AC is grateful to Raoul Röntsch and Vajravelu Ravindran for useful discussions. AC is also indebted to Andreas von Manteuffel for the help regarding the generation of the shift identities in `Reduze2` [55, 56]. AC has been supported by the Italian Ministry of Universities and Research through Grant No. PRIN 2022BCXSW9. The work of EC is funded by the ERC grant 101043686 'LoCoMotive'.

Data Availability Statement. This article has associated data in a data repository. Available at https://doi.org/10.5281/zenodo.14809205.

Code Availability Statement. This article has associated code in a code repository. Available at https://doi.org/10.5281/zenodo.14809205.

References

[1] CMS collaboration, *Search for high-mass diphoton resonances in proton–proton collisions at 13 TeV and combination with 8 TeV search*, *Phys. Lett. B* **767** (2017) 147 [arXiv:1609.02507] [INSPIRE].

[2] ATLAS collaboration, *Search for new phenomena in high-mass diphoton final states using 37 fb^{-1} of proton–proton collisions collected at $\sqrt{s} = 13$ TeV with the ATLAS detector*, *Phys. Lett. B* **775** (2017) 105 [arXiv:1707.04147] [INSPIRE].

[3] CDF collaboration, *Measurement of the Cross Section for Prompt Isolated Diphoton Production Using the Full CDF Run II Data Sample*, *Phys. Rev. Lett.* **110** (2013) 101801 [arXiv:1212.4204] [INSPIRE].

[4] D0 collaboration, *Measurement of the Differential Cross Sections for Isolated Direct Photon Pair Production in $p\bar{p}$ Collisions at $\sqrt{s} = 1.96$ TeV*, *Phys. Lett. B* **725** (2013) 6 [arXiv:1301.4536] [INSPIRE].

[5] CMS collaboration, *Measurement of the Production Cross Section for Pairs of Isolated Photons in pp collisions at $\sqrt{s} = 7$ TeV*, *JHEP* **01** (2012) 133 [arXiv:1110.6461] [INSPIRE].

[6] CMS collaboration, *Measurement of Differential Cross Sections for the Production of a Pair of Isolated Photons in pp Collisions at $\sqrt{s} = 7$ TeV*, *Eur. Phys. J. C* **74** (2014) 3129 [arXiv:1405.7225] [INSPIRE].

[7] ATLAS collaboration, *Observation of a new particle in the search for the Standard Model Higgs boson with the ATLAS detector at the LHC*, *Phys. Lett. B* **716** (2012) 1 [arXiv:1207.7214] [INSPIRE].

JHEP12(2025)106

[8] CMS collaboration, *Observation of a New Boson at a Mass of 125 GeV with the CMS Experiment at the LHC*, *Phys. Lett. B* **716** (2012) 30 [arXiv:1207.7235] [INSPIRE].

[9] T. Binoth, J.P. Guillet, E. Pilon and M. Werlen, *A Full next-to-leading order study of direct photon pair production in hadronic collisions*, *Eur. Phys. J. C* **16** (2000) 311 [hep-ph/9911340] [INSPIRE].

[10] S. Catani et al., *Diphoton production at hadron colliders: a fully-differential QCD calculation at NNLO*, *Phys. Rev. Lett.* **108** (2012) 072001 [*Erratum ibid.* **117** (2016) 089901] [arXiv:1110.2375] [INSPIRE].

[11] J.M. Campbell, R.K. Ellis, Y. Li and C. Williams, *Predictions for diphoton production at the LHC through NNLO in QCD*, *JHEP* **07** (2016) 148 [arXiv:1603.02663] [INSPIRE].

[12] S. Catani et al., *Diphoton production at the LHC: a QCD study up to NNLO*, *JHEP* **04** (2018) 142 [arXiv:1802.02095] [INSPIRE].

[13] R. Schuermann et al., *NNLO Photon Production with Realistic Photon Isolation*, *PoS* **LL2022** (2022) 034 [arXiv:2208.02669] [INSPIRE].

[14] M. Grazzini, S. Kallweit and M. Wiesemann, *Fully differential NNLO computations with MATRIX*, *Eur. Phys. J. C* **78** (2018) 537 [arXiv:1711.06631] [INSPIRE].

[15] D.A. Dicus and S.S.D. Willenbrock, *Photon Pair Production and the Intermediate Mass Higgs Boson*, *Phys. Rev. D* **37** (1988) 1801 [INSPIRE].

[16] V. Del Duca, W.B. Kilgore and F. Maltoni, *Multiphoton amplitudes for next-to-leading order QCD*, *Nucl. Phys. B* **566** (2000) 252 [hep-ph/9910253] [INSPIRE].

[17] C. Anastasiou, E.W.N. Glover and M.E. Tejeda-Yeomans, *Two loop QED and QCD corrections to massless fermion boson scattering*, *Nucl. Phys. B* **629** (2002) 255 [hep-ph/0201274] [INSPIRE].

[18] V. Del Duca, F. Maltoni, Z. Nagy and Z. Trocsanyi, *QCD radiative corrections to prompt diphoton production in association with a jet at hadron colliders*, *JHEP* **04** (2003) 059 [hep-ph/0303012] [INSPIRE].

[19] F. Caola, A. Von Manteuffel and L. Tancredi, *Diphoton Amplitudes in Three-Loop Quantum Chromodynamics*, *Phys. Rev. Lett.* **126** (2021) 112004 [arXiv:2011.13946] [INSPIRE].

[20] H.A. Chawdhry, M. Czakon, A. Mitov and R. Poncelet, *Two-loop leading-color helicity amplitudes for three-photon production at the LHC*, *JHEP* **06** (2021) 150 [arXiv:2012.13553] [INSPIRE].

[21] B. Agarwal, F. Buccioni, A. von Manteuffel and L. Tancredi, *Two-loop leading colour QCD corrections to $q\bar{q} \to \gamma\gamma g$ and $qg \to \gamma\gamma q$*, *JHEP* **04** (2021) 201 [arXiv:2102.01820] [INSPIRE].

[22] H.A. Chawdhry, M. Czakon, A. Mitov and R. Poncelet, *Two-loop leading-colour QCD helicity amplitudes for two-photon plus jet production at the LHC*, *JHEP* **07** (2021) 164 [arXiv:2103.04319] [INSPIRE].

[23] B. Agarwal, F. Buccioni, A. von Manteuffel and L. Tancredi, *Two-Loop Helicity Amplitudes for Diphoton Plus Jet Production in Full Color*, *Phys. Rev. Lett.* **127** (2021) 262001 [arXiv:2105.04585] [INSPIRE].

[24] M. Becchetti et al., *Full top-quark mass dependence in diphoton production at NNLO in QCD*, *Phys. Lett. B* **848** (2024) 138362 [arXiv:2308.10885] [INSPIRE].

[25] M. Becchetti et al., *Two-loop form factors for diphoton production in quark annihilation channel with heavy quark mass dependence*, *JHEP* **12** (2023) 105 [arXiv:2308.11412] [INSPIRE].

JHEP12(2025)106

[26] Z. Bern, A. De Freitas and L.J. Dixon, *Two loop amplitudes for gluon fusion into two photons*, *JHEP* **09** (2001) 037 [hep-ph/0109078] [INSPIRE].

[27] H.A. Chawdhry, M. Czakon, A. Mitov and R. Poncelet, *NNLO QCD corrections to diphoton production with an additional jet at the LHC*, *JHEP* **09** (2021) 093 [arXiv:2105.06940] [INSPIRE].

[28] Z. Bern, L.J. Dixon and C. Schmidt, *Isolating a light Higgs boson from the diphoton background at the CERN LHC*, *Phys. Rev. D* **66** (2002) 074018 [hep-ph/0206194] [INSPIRE].

[29] P. Bargiela, F. Caola, A. von Manteuffel and L. Tancredi, *Three-loop helicity amplitudes for diphoton production in gluon fusion*, *JHEP* **02** (2022) 153 [arXiv:2111.13595] [INSPIRE].

[30] F. Maltoni, M.K. Mandal and X. Zhao, *Top-quark effects in diphoton production through gluon fusion at next-to-leading order in QCD*, *Phys. Rev. D* **100** (2019) 071501 [arXiv:1812.08703] [INSPIRE].

[31] L. Chen et al., *Photon pair production in gluon fusion: top quark effects at NLO with threshold matching*, *JHEP* **04** (2020) 115 [arXiv:1911.09314] [INSPIRE].

[32] T. Peraro and L. Tancredi, *Physical projectors for multi-leg helicity amplitudes*, *JHEP* **07** (2019) 114 [arXiv:1906.03298] [INSPIRE].

[33] T. Peraro and L. Tancredi, *Tensor decomposition for bosonic and fermionic scattering amplitudes*, *Phys. Rev. D* **103** (2021) 054042 [arXiv:2012.00820] [INSPIRE].

[34] L. Chen, *A prescription for projectors to compute helicity amplitudes in D dimensions*, *Eur. Phys. J. C* **81** (2021) 417 [arXiv:1904.00705] [INSPIRE].

[35] J.A.M. Vermaseren, *New features of FORM*, math-ph/0010025 [INSPIRE].

[36] P. Maierhöfer, J. Usovitsch and P. Uwer, *Kira — A Feynman integral reduction program*, *Comput. Phys. Commun.* **230** (2018) 99 [arXiv:1705.05610] [INSPIRE].

[37] J. Klappert, F. Lange, P. Maierhöfer and J. Usovitsch, *Integral reduction with Kira 2.0 and finite field methods*, *Comput. Phys. Commun.* **266** (2021) 108024 [arXiv:2008.06494] [INSPIRE].

[38] K.G. Chetyrkin, A.L. Kataev and F.V. Tkachov, *Higher Order Corrections to* $\sigma_{\rm tot}(e^+e^- \to \text{Hadrons})$ *in Quantum Chromodynamics*, *Phys. Lett. B* **85** (1979) 277 [INSPIRE].

[39] K.G. Chetyrkin and F.V. Tkachov, *Integration by parts: the algorithm to calculate* β*-functions in 4 loops*, *Nucl. Phys. B* **192** (1981) 159 [INSPIRE].

[40] S. Caron-Huot and J.M. Henn, *Iterative structure of finite loop integrals*, *JHEP* **06** (2014) 114 [arXiv:1404.2922] [INSPIRE].

[41] M. Becchetti and R. Bonciani, *Two-Loop Master Integrals for the Planar QCD Massive Corrections to Di-photon and Di-jet Hadro-production*, *JHEP* **01** (2018) 048 [arXiv:1712.02537] [INSPIRE].

[42] A. A H, E. Chaubey and H.-S. Shao, *Two-loop massive QCD and QED helicity amplitudes for light-by-light scattering*, *JHEP* **03** (2024) 121 [arXiv:2312.16966] [INSPIRE].

[43] X. Xu and L.L. Yang, *Towards a new approximation for pair-production and associated-production of the Higgs boson*, *JHEP* **01** (2019) 211 [arXiv:1810.12002] [INSPIRE].

[44] T. Ahmed, E. Chaubey, M. Kaur and S. Maggio, *Two-loop non-planar four-point topology with massive internal loop*, *JHEP* **05** (2024) 064 [arXiv:2402.07311] [INSPIRE].

JHEP12(2025)106

[45] T. Ahmed, A. Chakraborty, E. Chaubey and M. Kaur, *Ancillary files for "Two-loop helicity amplitudes for diphoton production with massive quark loop"*, (2025), DOI:10.5281/zenodo.14809205.

[46] G. 't Hooft and M.J.G. Veltman, *Regularization and Renormalization of Gauge Fields*, *Nucl. Phys. B* **44** (1972) 189 [INSPIRE].

[47] T. Ahmed et al., *Polarised Amplitudes and Soft-Virtual Cross Sections for $b\bar{b} \to ZH$ at NNLO in QCD*, *JHEP* **01** (2020) 030 [arXiv:1910.06347] [INSPIRE].

[48] F. Caola et al., *Three-Loop Gluon Scattering in QCD and the Gluon Regge Trajectory*, *Phys. Rev. Lett.* **128** (2022) 212001 [arXiv:2112.11097] [INSPIRE].

[49] P. Bargiela, A. Chakraborty and G. Gambuti, *Three-loop helicity amplitudes for photon+jet production*, *Phys. Rev. D* **107** (2023) L051502 [arXiv:2212.14069] [INSPIRE].

[50] T. Binoth, E.W.N. Glover, P. Marquard and J.J. van der Bij, *Two loop corrections to light by light scattering in supersymmetric QED*, *JHEP* **05** (2002) 060 [hep-ph/0202266] [INSPIRE].

[51] T. Ahmed, J. Henn and B. Mistlberger, *Four-particle scattering amplitudes in QCD at NNLO to higher orders in the dimensional regulator*, *JHEP* **12** (2019) 177 [arXiv:1910.06684] [INSPIRE].

[52] F. Caola et al., *Three-loop helicity amplitudes for quark-gluon scattering in QCD*, *JHEP* **12** (2022) 082 [arXiv:2207.03503] [INSPIRE].

[53] L.J. Dixon, *Calculating scattering amplitudes efficiently*, in the proceedings of the *Theoretical Advanced Study Institute in Elementary Particle Physics (TASI 95)*, Boulder, U.S.A., June 04–30 (1995) [hep-ph/9601359] [INSPIRE].

[54] P. Nogueira, *Automatic Feynman Graph Generation*, *J. Comput. Phys.* **105** (1993) 279 [INSPIRE].

[55] C. Studerus, *Reduze — Feynman integral reduction in C++*, *Comput. Phys. Commun.* **181** (2010) 1293 [arXiv:0912.2546] [INSPIRE].

[56] A. von Manteuffel and C. Studerus, *Reduze 2 — Distributed Feynman Integral Reduction*, arXiv:1201.4330 [INSPIRE].

[57] R.N. Lee, *Presenting LiteRed: a tool for the Loop InTEgrals REDuction*, arXiv:1212.2685 [INSPIRE].

[58] S. Laporta, *High-precision calculation of multiloop Feynman integrals by difference equations*, *Int. J. Mod. Phys. A* **15** (2000) 5087 [hep-ph/0102033] [INSPIRE].

[59] T. Peraro, *FiniteFlow: multivariate functional reconstruction using finite fields and dataflow graphs*, *JHEP* **07** (2019) 031 [arXiv:1905.08019] [INSPIRE].

[60] A. von Manteuffel and R.M. Schabinger, *A novel approach to integration by parts reduction*, *Phys. Lett. B* **744** (2015) 101 [arXiv:1406.4513] [INSPIRE].

[61] A. von Manteuffel and R.M. Schabinger, *Quark and gluon form factors to four-loop order in QCD: the N_f^3 contributions*, *Phys. Rev. D* **95** (2017) 034030 [arXiv:1611.00795] [INSPIRE].

[62] T. Peraro, *Scattering amplitudes over finite fields and multivariate functional reconstruction*, *JHEP* **12** (2016) 030 [arXiv:1608.01902] [INSPIRE].

[63] J.M. Henn, *Multiloop integrals in dimensional regularization made simple*, *Phys. Rev. Lett.* **110** (2013) 251601 [arXiv:1304.1806] [INSPIRE].

[64] W. Magnus, *On the exponential solution of differential equations for a linear operator*, *Commun. Pure Appl. Math.* **7** (1954) 649 [INSPIRE].

JHEP12(2025)106

[65] M. Becchetti et al., *Analytic two-loop amplitudes for $q\bar{q} \to \gamma\gamma$ and $gg \to \gamma\gamma$ mediated by a heavy-quark loop*, *JHEP* **06** (2025) 033 [arXiv:2502.00118] [INSPIRE].

[66] J. Vollinga and S. Weinzierl, *Numerical evaluation of multiple polylogarithms*, *Comput. Phys. Commun.* **167** (2005) 177 [hep-ph/0410259] [INSPIRE].

[67] S. Badger, E. Chaubey, H.B. Hartanto and R. Marzucca, *Two-loop leading colour QCD helicity amplitudes for top quark pair production in the gluon fusion channel*, *JHEP* **06** (2021) 163 [arXiv:2102.13450] [INSPIRE].

[68] E. Chaubey, *Master integrals contributing to two-loop leading colour QCD helicity amplitudes for top-quark pair production in the gluon fusion channel*, *SciPost Phys. Proc.* **7** (2022) 001 [arXiv:2110.15844] [INSPIRE].

[69] S. Catani, *The singular behavior of QCD amplitudes at two loop order*, *Phys. Lett. B* **427** (1998) 161 [hep-ph/9802439] [INSPIRE].

[70] G.F. Sterman and M.E. Tejeda-Yeomans, *Multiloop amplitudes and resummation*, *Phys. Lett. B* **552** (2003) 48 [hep-ph/0210130] [INSPIRE].

[71] S.M. Aybat, L.J. Dixon and G.F. Sterman, *The Two-loop anomalous dimension matrix for soft gluon exchange*, *Phys. Rev. Lett.* **97** (2006) 072001 [hep-ph/0606254] [INSPIRE].

[72] S.M. Aybat, L.J. Dixon and G.F. Sterman, *The Two-loop soft anomalous dimension matrix and resummation at next-to-next-to leading pole*, *Phys. Rev. D* **74** (2006) 074004 [hep-ph/0607309] [INSPIRE].

[73] T. Becher and M. Neubert, *Infrared singularities of scattering amplitudes in perturbative QCD*, *Phys. Rev. Lett.* **102** (2009) 162001 [*Erratum ibid.* **111** (2013) 199905] [arXiv:0901.0722] [INSPIRE].

[74] T. Becher and M. Neubert, *On the Structure of Infrared Singularities of Gauge-Theory Amplitudes*, *JHEP* **06** (2009) 081 [*Erratum ibid.* **11** (2013) 024] [arXiv:0903.1126] [INSPIRE].

[75] L.J. Dixon, *Matter Dependence of the Three-Loop Soft Anomalous Dimension Matrix*, *Phys. Rev. D* **79** (2009) 091501 [arXiv:0901.3414] [INSPIRE].

[76] E. Gardi and L. Magnea, *Factorization constraints for soft anomalous dimensions in QCD scattering amplitudes*, *JHEP* **03** (2009) 079 [arXiv:0901.1091] [INSPIRE].

[77] E. Gardi and L. Magnea, *Infrared singularities in QCD amplitudes*, *Nuovo Cim. C* **32N5-6** (2009) 137 [arXiv:0908.3273] [INSPIRE].

[78] O. Almelid, C. Duhr and E. Gardi, *Three-loop corrections to the soft anomalous dimension in multileg scattering*, *Phys. Rev. Lett.* **117** (2016) 172002 [arXiv:1507.00047] [INSPIRE].

[79] S. Catani, S. Dittmaier and Z. Trocsanyi, *One loop singular behavior of QCD and SUSY QCD amplitudes with massive partons*, *Phys. Lett. B* **500** (2001) 149 [hep-ph/0011222] [INSPIRE].

[80] A. Ferroglia, M. Neubert, B.D. Pecjak and L.L. Yang, *Two-loop divergences of scattering amplitudes with massive partons*, *Phys. Rev. Lett.* **103** (2009) 201601 [arXiv:0907.4791] [INSPIRE].

[81] A. Ferroglia, M. Neubert, B.D. Pecjak and L.L. Yang, *Two-loop divergences of massive scattering amplitudes in non-abelian gauge theories*, *JHEP* **11** (2009) 062 [arXiv:0908.3676] [INSPIRE].

[82] A. Mitov, G.F. Sterman and I. Sung, *The Massive Soft Anomalous Dimension Matrix at Two Loops*, *Phys. Rev. D* **79** (2009) 094015 [arXiv:0903.3241] [INSPIRE].

JHEP12(2025)106

[83] A. Mitov, G.F. Sterman and I. Sung, *Computation of the Soft Anomalous Dimension Matrix in Coordinate Space*, *Phys. Rev. D* **82** (2010) 034020 [arXiv:1005.4646] [INSPIRE].

[84] Z.L. Liu and N. Schalch, *Infrared Singularities of Multileg QCD Amplitudes with a Massive Parton at Three Loops*, *Phys. Rev. Lett.* **129** (2022) 232001 [arXiv:2207.02864] [INSPIRE].

[85] M. Steinhauser, *Results and techniques of multiloop calculations*, *Phys. Rept.* **364** (2002) 247 [hep-ph/0201075] [INSPIRE].

[86] G.P. Korchemsky and A.V. Radyushkin, *Renormalization of the Wilson Loops Beyond the Leading Order*, *Nucl. Phys. B* **283** (1987) 342 [INSPIRE].

[87] S. Moch, J.A.M. Vermaseren and A. Vogt, *The three loop splitting functions in QCD: the Nonsinglet case*, *Nucl. Phys. B* **688** (2004) 101 [hep-ph/0403192] [INSPIRE].

[88] A. Vogt, S. Moch and J.A.M. Vermaseren, *The Three-loop splitting functions in QCD: the Singlet case*, *Nucl. Phys. B* **691** (2004) 129 [hep-ph/0404111] [INSPIRE].

[89] R. Brüser, A. Grozin, J.M. Henn and M. Stahlhofen, *Matter dependence of the four-loop QCD cusp anomalous dimension: from small angles to all angles*, *JHEP* **05** (2019) 186 [arXiv:1902.05076] [INSPIRE].

[90] J.M. Henn, G.P. Korchemsky and B. Mistlberger, *The full four-loop cusp anomalous dimension in $\mathcal{N} = 4$ super Yang-Mills and QCD*, *JHEP* **04** (2020) 018 [arXiv:1911.10174] [INSPIRE].

[91] A. von Manteuffel, E. Panzer and R.M. Schabinger, *Cusp and collinear anomalous dimensions in four-loop QCD from form factors*, *Phys. Rev. Lett.* **124** (2020) 162001 [arXiv:2002.04617] [INSPIRE].

[92] V. Ravindran, J. Smith and W.L. van Neerven, *Two-loop corrections to Higgs boson production*, *Nucl. Phys. B* **704** (2005) 332 [hep-ph/0408315] [INSPIRE].

[93] S. Moch, J.A.M. Vermaseren and A. Vogt, *The Quark form-factor at higher orders*, *JHEP* **08** (2005) 049 [hep-ph/0507039] [INSPIRE].

[94] S. Moch, J.A.M. Vermaseren and A. Vogt, *Three-loop results for quark and gluon form-factors*, *Phys. Lett. B* **625** (2005) 245 [hep-ph/0508055] [INSPIRE].

[95] B. Agarwal, A. von Manteuffel, E. Panzer and R.M. Schabinger, *Four-loop collinear anomalous dimensions in QCD and N=4 super Yang-Mills*, *Phys. Lett. B* **820** (2021) 136503 [arXiv:2102.09725] [INSPIRE].

[96] F. Caola et al., *Three-loop helicity amplitudes for four-quark scattering in massless QCD*, *JHEP* **10** (2021) 206 [arXiv:2108.00055] [INSPIRE].

[97] X. Liu, Y.-Q. Ma and C.-Y. Wang, *A Systematic and Efficient Method to Compute Multi-loop Master Integrals*, *Phys. Lett. B* **779** (2018) 353 [arXiv:1711.09572] [INSPIRE].

[98] X. Liu and Y.-Q. Ma, *AMFlow: a Mathematica package for Feynman integrals computation via auxiliary mass flow*, *Comput. Phys. Commun.* **283** (2023) 108565 [arXiv:2201.11669] [INSPIRE].

[99] J. Davies, G. Mishima, K. Schönwald and M. Steinhauser, *Analytic approximations of $2 \to 2$ processes with massive internal particles*, *JHEP* **06** (2023) 063 [arXiv:2302.01356] [INSPIRE].

JHEP12(2025)106